

Carleman-lattice-Boltzmann quantum circuit with matrix access oracles

Claudio Sanavio,¹ William A. Simon,² Alex Ralli,² Peter Love,² and Sauro Succi^{1,2}

¹*Fondazione Istituto Italiano di Tecnologia
Center for Life Nano-Neuroscience at la Sapienza
Viale Regina Elena 291, 00161 Roma, Italy*

²*Department of Physics and Astronomy, Tufts University
574 Boston Avenue, Medford, MA 02155, USA*

(*Electronic mail: claudio.sanavio@iit.it)

(Dated: January 7, 2025)

We apply Carleman linearization of the Lattice Boltzmann (CLB) representation of fluid flows to quantum emulate the dynamics of a 2D Kolmogorov-like flow. We assess the accuracy of the result and find a relative error of the order of 10^{-3} with just two Carleman iterates, for a range of the Reynolds number up to a few hundreds. We first define a gate-based quantum circuit for the implementation of the CLB method and then exploit the sparse nature of the CLB matrix to build a quantum circuit based on block-encoding techniques which makes use of matrix oracles. It is shown that the gate complexity of the algorithm is thereby dramatically reduced, from exponential to quadratic. However, due to the need of employing up to seven ancilla qubits, the probability of success of the corresponding circuit for a single time step is too low to enable multi-step time evolution. Several possible directions to circumvent this problem are briefly outlined.

I. INTRODUCTION

The Lattice Boltzmann method (LBM) has proved to be an important tool for the simulation of fluid dynamics with a wide range of applications in the physics of fluids and allied disciplines¹⁻⁶.

The basic equations of classical fluid motion are known for over two centuries, after the seminal work of Louis Navier in France and Gabriel Stokes in UK. In essence, they are Newton's equation in reverse, $ma = F$, as applied to a finite volume of fluid. For the case of an incompressible flow (constant density), they take the following form:

$$\partial_t \vec{u} + \vec{u} \cdot \nabla \vec{u} = -\nabla p + \nu \Delta \vec{u} \quad (1)$$

where $\vec{u} = \vec{u}(\vec{x}, t)$ is the space-time dependent flow field (vector), p is the pressure and ν the kinematic viscosity. Incompressibility forces the solenoidal condition

$$\nabla \cdot \vec{u} = 0. \quad (2)$$

Despite their innocent appearance, the Navier-Stokes equations (NSE) hide a Pandora's box of complexity, from the dripping droplets in the kitchen faucet, all the way up to geophysical flows, including extreme events such as tornadoes and hurricanes, a very hot topic in these modern times of environmental concerns.

The key mechanism is deceptively simple: the nonlinear and nonlocal term $\vec{u} \cdot \nabla \vec{u}$ fuels a cascade of energy from large to small scales, virtually dissipation-free. Dissipation enters stage only once the fluid structures become small enough for dissipation to take over the nonlinear energy transfer. The crossover scale, named after the russian polymath Andreij Kolmogorov is given by $L_k = L/Re^{3/4}$ where

$$Re = \frac{UL}{\nu} \quad (3)$$

is the so-called Reynolds number, the effective measure of Nonlinearity versus Dissipation. In the above, L is the macroscopic scale of the fluid, U its typical macroscopic velocity and ν the viscosity of the fluid.

The Reynolds number is generally pretty large; an ordinary car features $Re \sim 10^7$ and that's where complexity steps in: the number of active structures in a flow at Reynolds Re scales like $(L/L_k)^3 \sim Re^{9/4}$ and computing such flow over a time span $T = O(L)$ involves $O(Re^3)$ operations, the computational complexity of fluid turbulence.

For a car this means circa 10^{24} floating-point operations per simulation (we count about 1000 operations each grid site and time step), a run that a perfect Exaflop computer (10^{18} Flops/second) would complete in about two weeks. Hence we may feel confident than in a few years, classical Exascale computers may "compute away" a fully-fledged car design. Not so for weather forecasting, where Reynolds numbers increase by another three to five orders of magnitude. Whence the ceaseless race to new and better computational methods. Including, lately quantum computing⁷.

Quantum computers may offer a solution to the complexity problem, since the dimension of Hilbert's space scales exponentially with the number of qubits. In his 1982 paper "Simulating physics with computers"⁸, Richard Feynman argued that "nature isn't classical", hence if we want to simulate nature at a fundamental level we'd better use quantum computers.

Feynman invoked the QQ approach to scientific computing: quantum computers for quantum physics. Fluid turbulence however is (mostly) classical, hence a CC approach (classical computers for classical systems) appears reasonable after all. Yet, given the large Reynolds numbers encountered in science and engineering, the computational complexity Re^3 is steep, hence it is of decided interest to investigate whether a QC approach (quantum computers for classical physics) may offer a quantum advantage.

In principle the potential is huge: since qubits offer logarithmic scaling for the $Re^{9/4}$ complexity, $\frac{9}{4}\log_2(Re)$ qubits are in principle sufficient to represent a given Reynolds number Re . This would be mind-boggling with potentially revolutionary perspectives: with 10 to 100 physical qubits for each logical one, local weather forecast ($Re \sim 10^{10}$) would become available with less than thousands to ten thousands qubits.

However, realizing this blue sky scenario faces a sequence of steep challenges: first, one must devise a quantum algorithm for fluids, second it must show logarithmic scaling of its computational complexity, third it must run efficiently on actual quantum hardware. In the following, we take a very optimistic stance, namely that efficient quantum hardware will eventually become available, far from foregone given the levels of quantum noise in current day quantum hardware. Hence, in the following, we focus on the task of devising a quantum computing algorithm for the fluid equations.

The task of simulating classical fluid dynamics on quantum computers requires the ability to handle nonlinearity and dissipation. Quantum computers behave according to the laws of quantum mechanics, which are both linear and non-dissipative. Many strategies have been proposed in the recent years to handle both items above⁹, but it appears fair to say that, to date, none of them has led to a viable quantum algorithm for fluids, meaning by this an algorithm that can be run efficiently on actual quantum hardware.

This paper follows in the wake of a series of works on various approaches to implement a quantum Lattice Boltzmann algorithm^{10,11}, and on the Carleman linearization procedure¹²⁻¹⁴. In our previous work, we found that the Carleman linearization (CL) is able to approximate nonlinear fluid dynamics with an error that decays exponentially with the number of Carleman iterations¹⁵, a result consistent with the findings in Refs. ^{16,17}. In particular, when applied to the Lattice Boltzmann model, the Carleman procedure shows an excellent convergence: with a second truncation level, CL represents the exact dynamics of 1D model¹², and a relative error in the order of 10^{-3} for a 2D Kolmogorov-like flow^{11,13}. With a truncation level at third order, CL exhibits a relative error of the same order of magnitude as the intrinsic error of Lattice Boltzmann¹⁸.

These favourable properties motivated the search of a Carleman Lattice Boltzmann (CLB) quantum algorithm. In¹¹, an algorithm is developed based on linear combination of unitaries (LCU) to implement the Carleman evolution. For a single timestep evolution, the gate complexity of the system was fixed to few thousands CNOTs, regardless of the number of lattice sites. However, the implementation of a multiple timestep simulation requires to measure and reinitialize the circuit at each timestep, a process that would require an exponential number of measurements. Conversely, the multi-time step circuit led to a gate complexity that scales exponentially with the number of qubits. In¹⁸, the authors calculated the gate complexity of a Carleman Lattice Boltzmann algorithm and showed that it can be made linear in time and logarithmic with the number of qubits, under the assumption that one is able to prepare an efficient oracle that embeds the Carleman evolution.

In this paper, we describe an efficient preparation of the circuit that implements the multiple-time step Carleman Lattice Boltzmann evolution. Our approach is based upon a block-encoding technique, and we show it is a potential way out of the problem, since it reduces the gate complexity from exponential to polynomial.

In Sec. II, we describe the CL procedure that we use to transform the nonlinear problem into a linear one. In Sec. III we apply CL to the LB for the case of a 2D Kolmogorov-like flow and we discuss the convergence of the CLB algorithm. In Sec. IV we discuss the potential obstacles to an implementation of the CLB algorithm. In Sec. V we describe the block-encoding technique as applied to the CLB framework and provide the explicit form of the quantum circuit, along with an analysis of its performance. In Sec. VI we draw preliminary conclusions and portray a few promising directions for future developments.

II. CARLEMAN LINEARIZATION

The basic idea of Carleman linearization is to embed a finite-dimensional non-linear problem into an infinite-dimensional linear one. The idea is readily explained by means of the zero-dimensional logistic equation:

$$\dot{u} = -u(1 - Ru), \quad (4)$$

$$u(0) = u_0 \quad (5)$$

where u is a single variable (zero spatial dimensions) and R measures the strength of the nonlinearity.

The Carleman embedding consists in renaming $u_1 \equiv u$ and $u_2 \equiv u^2$, so that the logistic equation turns into $\dot{u}_1 = -u_1 + Ru_2$, which is linear but open, since u_2 is a new independent variable. The equation for u_2 is easily found by multiplying Eq. (4) by u , to obtain $\dot{u}_2 = -2(u_2 - Ru_3)$ where $u_3 \equiv u^3$. The trick is now clear, at each step k one generates an open equation for u_k involving u_{k+1} , thus leading to an infinite Carleman chain. Eventually, this infinite chain can be solved analytically to recover the

exact solution, but in general one looks for a finite-order truncation, hopefully providing a reasonably accurate approximation. By truncating at a given order K , one obtains:

$$\dot{u}_k = -k(u_k - Ru_{k+1}), \quad k = 1, \dots, K-1 \quad (6)$$

$$\dot{u}_K = -Ku_K, \quad (7)$$

with initial conditions $u_k(0) = u_0^k$.

The bet is to achieve reasonable accuracy within a small number of iterations along the Carleman ladder. For a thorough analysis of the Carleman linearization applied to the logistic equation we refer to¹⁴.

The idea is elegant but faces a number of issues when applied to multi-dimensional problems. To appreciate the point, let us consider the Navier-Stokes equations, after spatial differencing and Euler time-marching:

$$u(t+h) = (I+Lh)u(t) + hRe Q u(t)u(t) \equiv Au + Bu \otimes u \quad (8)$$

where u is the state vector consisting of $N = O(G)$ variables in a discrete grid of G lattice sites. In the above, I is the identity, L is the discretized Laplacian, Re is the Reynolds number and Q is the discretized quadratic advection operator.

For notational simplicity we have set $A = (I+hL)$ and $B = hReQ$, where $A \equiv A_{ij}$ is a rank-2 sparse matrix and $B \equiv B_{ijk}$ is also a sparse matrix of rank 3. For simplicity, we have left out pressure, hence the above scheme applies to the Burgers equation.

Call $U_2 \equiv u \otimes u$ and similarly U_3, U_4, \dots , the Burgers becomes a linear, open equation.

$$U_1(t+h) = AU_1(t) + BU_2(t). \quad (9)$$

The equation for U_2 is readily obtained:

$$U_2(t+h) = A^{\otimes 2}U_2(t) + Re(A \otimes B + B \otimes A)U_3(t) + B^{\otimes 2}U_4(t). \quad (10)$$

The above set of equations can be written in terms of a linear system

$$\begin{pmatrix} U_1 \\ U_2 \\ \vdots \end{pmatrix} (t+h) = \mathcal{C} \begin{pmatrix} U_1 \\ U_2 \\ \vdots \end{pmatrix} (t), \quad (11)$$

where \mathcal{C} is the Carleman matrix. The lowest possible truncation ($K=2$) of the above system leaves us with the following system:

$$U_1(t+h) = AU_1(t) + BU_2(t) \quad (12)$$

$$U_2(t+h) = A^{\otimes 2}U_2(t) \quad (13)$$

Hence, the Carleman matrix features two rows: $[A, B]$ and $[0, A^{\otimes 2}]$. Note that in general, U_2 contains non local terms of the form $u_i u_j$. Hence the number of Carleman variables at the second order truncation is $N_2 = O(G+G^2)$.

The efficiency of the procedure clearly depends on the level at which one truncates the Carleman hierarchy, which in turn depends on the strength of the nonlinearity and the desired time of evolution. In general, it is clear that each increasing step of the ladder entails a corresponding increase of non-locality and a combinatorial increase of dimensionality, meaning by this the number of Carleman variables. This compounds with the fact that in a quantum computer it is highly unpractical to measure the state $u(t+h)$, since this procedure has complexity $O(N_2^2)$. One way out is to use telescopic time marching, namely go from $u(0)$ to $u(t+T)$, $T = N_t h$, in a single "long-jump" update straddling across N_t "small" steps. This clearly aggravates the non-locality problem, since the product $u_i(t+T)u_j(t+T)$ displays non-zero components across the entire grid (as soon as T is comparable with the linear size L of the domain).

Details may change depending on the specific procedure, but these general trends remain: transforming the nonlinearity away comes with a major computational burden. Detailed experiments have shown that the Carleman-Navier-Stokes procedure exhibits very poor convergence even at moderate values of the Reynolds number. Typically, just a few steps with Carleman truncation below $K=4$ are found to incur errors well above 10 percent¹³.

III. CARLEMAN LATTICE BOLTZMANN

A much better convergence has been found when the Carleman procedure is applied to the Lattice Boltzmann (LB) equation:

$$f_p(\vec{x} + \vec{c}_p \Delta t, t + \Delta t) - f_p(\vec{x}, t) = -\omega [f_p(\vec{x}, t) - f_p^{eq}(\vec{x}, t)], \quad p = 1, \dots, b \quad (14)$$

where the discrete index p labels the discrete velocities \vec{c}_p and Δt is the timestep. The left side of the equation represents the *streaming* of the fluid towards the neighboring sites along the p -th direction. Streaming is a nonlocal and linear operation which is exact on a classical computer as it does not involve any floating-point operation since particles hop from one lattice site to the corresponding neighbor with no loss of information. The right side of the equation represents the *relaxation* towards the local equilibrium, and ω is inversely proportional to the relaxation time-scale. The parameter ω controls the LB fluid viscosity, hence the Reynolds number, according to

$$\nu = c_s^2 \left(\frac{1}{\omega} - \frac{1}{2} \right), \quad (15)$$

c_s being the lattice sound speed.

The relaxation step is local and nonlinear, the nonlinearity of the fluid equations being entirely described by the quadratic terms in the local equilibrium:

$$f_p^{eq} = w_p \left(1 + \vec{u}_p + \frac{1}{2} (|\vec{u}_p|^2 - |\vec{u}|^2) \right) \quad (16)$$

where $\vec{u}_p \equiv \frac{\vec{u} \cdot \vec{c}_p}{c_s}$, and w_p being a weight corresponding to the equilibrium distribution with no flow ($\vec{u} = 0$). The values of the weights w_p depend on the specific model, popular versions being the D2Q9 (two dimensions, 9 velocities) and the D3Q27 (three dimensions, 27 velocities). Those are represented in Fig. 1.

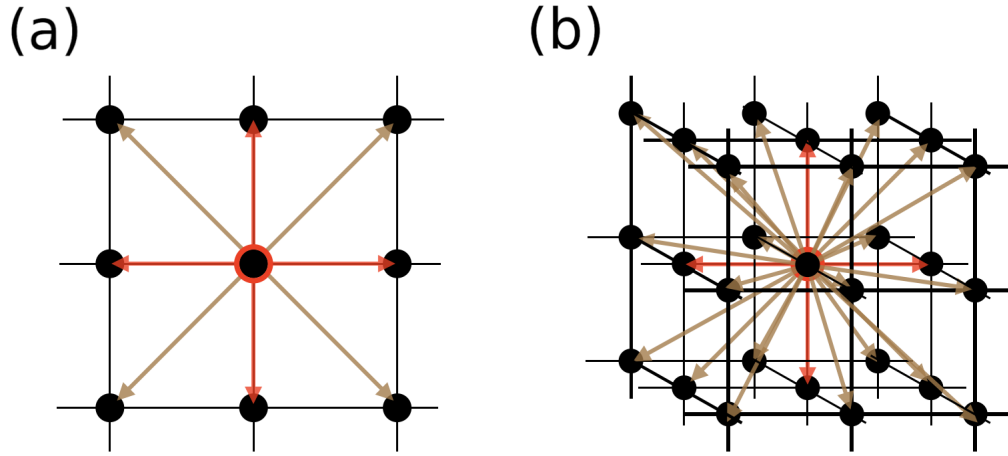


Figure 1. (a) The D2Q9 model with $3^2 = 9$ velocities pointing to the neighboring sites, and (b) the D3Q27 model with the $3^3 = 27$ velocities pointing to the neighboring sites in three-dimensions. They are generated by tensor product of the one-dimensional D1Q3 lattice with three discrete velocities $(-1, 0, +1)$. The 0-th velocity is represented by the red circle in the center of the lattice.

The Carleman Lattice Boltzmann (CLB) procedure consists in treating the second (and higher) order terms $f_{pq} = f_p f_q$, coming from the expansion of Eq. (16), as new variables and then defining their evolution following Eq. (14). This can be written as a linear system in the form

$$F(t + \Delta t) = \mathcal{C}F(t),$$

where $F(t)$ is the vector collecting the first f_p and second f_{pq} order terms at all lattice sites while \mathcal{C} is the Carleman matrix.

In the LB method, we can treat streaming and relaxation separately and the same holds true for the CLB method, namely:

$$\mathcal{C} = \mathcal{S}\mathcal{R}.$$

The streaming matrix \mathcal{S} is unitary, while the relaxation matrix \mathcal{R} is not, as it encodes the irreversible decay to the local equilibrium leading to emergent dissipation. Thus we can separate the two processes and apply streaming after relaxation.

The streaming operator for the D2Q9 model has been thoroughly investigated in¹¹, but being unitary, it does not entail the same burden as the implementation of the nonunitary operator \mathcal{R} .

In fact, it can be expressed by a circuit whose depth scales quadratically with the number of qubits, and a width that is twice the original¹⁹.

The CLB relaxation process, truncated at second order, turns into the following linear system

$$f_p(x + hc_p, t + h) = A_{pq} f_q(x, t) + B_{pqr} f_{qr}(x, t) \quad (17)$$

$$f_{pq}(x + hc_p, y + hc_q, t + h) = A_{pr} A_{qs} f_{rs}(x, y, t), \quad (18)$$

This allows to write the relaxation matrix over N lattice sites as

$$\mathcal{R}_N = \begin{pmatrix} 1_N \otimes A & \Delta \otimes B \\ 0 & 1_{N^2} \otimes A^{\otimes 2} \end{pmatrix}, \quad (19)$$

where the matrix Δ accounts for the locality of the relaxation process. Thus the non-null components $\Delta_{x,y} = \delta_{x,(N+1)y}$ with $x, y = 0, \dots, N-1$, couple together the local Carleman variables of first and second order. For notational simplicity, in the following the spatial indices will be denoted simply by i, j, k .

The matrix B gives the strength of the coupling between first and second order Carleman variables. Note that this is analogous to Eq. (12), but we have detailed the dependence on the position of the variables. The single lattice-site relaxation matrix for the D2Q9 model takes the form plotted in Fig. 2. The block in the upper-left side of the matrix is the b/w representation of the matrix A , which is a 9×9 full matrix. The large 81×81 matrix in the bottom-right side of the matrix represents the matrix B . Although this matrix has a sparsity $s = 81$, out of 90 rows and columns, it is worth to notice that its multiple lattice-sites version \mathcal{R}_N (Eq. (19)) has the same sparsity, regardless of the number of lattice sites N . For any LB model with b velocities, the sparsity of the Carleman relaxation matrix truncated at order τ is $s = b^\tau$.

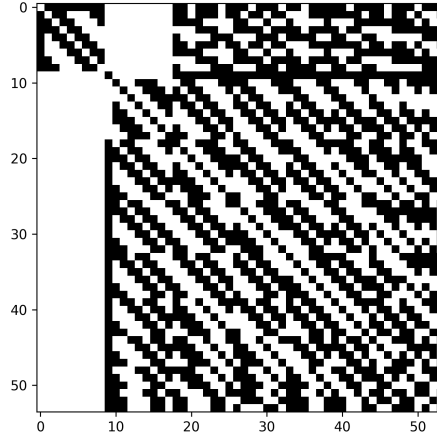


Figure 2. A black-and-white representation of the Carleman Lattice Boltzmann relaxation matrix \mathcal{R}_1 for a single lattice site for the D2Q9 model. In the white blocks, the value of \mathcal{R}_1 is 0.

Since dissipation is emergent and does not require any Laplacian, the nonlinear/linear ratio in this formulation amounts to comparing linear and quadratic terms in the local equilibria, which is simply given by the Mach number. This makes a huge difference as compared to Navier-Stokes since the Mach number is generally orders of magnitude smaller than the Reynolds number. Hence, LB presents a much smaller nonlinearity barrier to the Carleman procedure¹⁸. This intuition is indeed backed up by numerical experiments, which show excellent convergence of the CLB procedure. Even at second order truncation, flows with Reynolds number $O(100)$ exhibit relative errors of about 10^{-3} over hundreds of timesteps in the case of a 2D Kolmogorov-like flow¹¹ calculated on a 48×48 regular lattice, and simulated with lattice units $\Delta x = \Delta t = 1$ and $c_s = 1/\sqrt{3}$. In Fig. 3(a) we show the relative error ε of the CLB method for the three "max-med-min" points of the lattice where it reaches the maximum, median and minimum value.

In Fig. 3(b) we show the relative error averaged over the whole lattice $\langle \varepsilon \rangle$. The curves refer to different values of the Reynolds number, $\text{Re} \approx 30, 90, 550$ obtained by varying the parameter $\omega = 1, 1.5, 1.9$ respectively, with $|\vec{u}| \approx 0.1$, see Eqs. (15) and (3).

Much more systematic work is needed to assess whether the very encouraging convergence properties of the CLB procedure extend to more complex flows, such as high-Reynolds numbers in confined geometries. To this regard, it is important to observe that such an analysis can only be performed on a quantum computer, since the CLB procedure rapidly saturates the memory capacity of classical ones, due to the exponential growth of the number of Carleman variables with the grid size and the truncation level of the Carleman embedding.

In the following, we address precisely this issue.

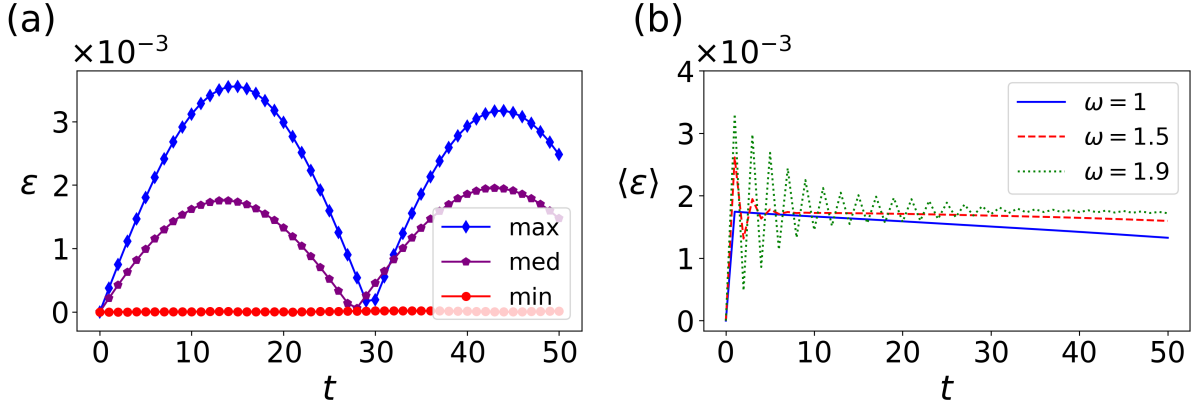


Figure 3. In (a) the relative error ε between the results obtained by LBM and by Carleman linearization truncated at second order for a Kolmogorov-like flow simulated on a 48×48 square lattice. The error is monitored at three points, where ε is maximum (blue diamonds), median (purple pentagons) and minimum (red circles). In (b) the error averaged over all the lattice sites for different values of ω .

IV. TOWARDS A QUANTUM CLB ALGORITHM

The development of a quantum CLB algorithm faces a number of challenges. In a nutshell, the main problem is that even the single-lattice site CLB matrix projects over the entire series $\{\sigma_i\}_i$ of tensor Pauli gates, obtained by all the possible combinations of tensor product between the three Pauli matrices and the identity. In Fig. 4(a) we plot the value s_i of the associated coefficients sorted in decreasing order. To evaluate the performance of the expansion we calculate the normalized Frobenius distance

$$d(\mathcal{R}_1, \Sigma_n) = \frac{\|\mathcal{R}_1 - \Sigma_n\|}{\|\mathcal{R}_1\|} \quad (20)$$

between the Carleman matrix \mathcal{R}_1 detailed in Eq. (19) and the matrix obtained by partial expansion of \mathcal{R}_1 with the most relevant n elements $\Sigma_n = \sum_{i=1}^n s_i \sigma_i$. We plot it in Fig. 4(b).

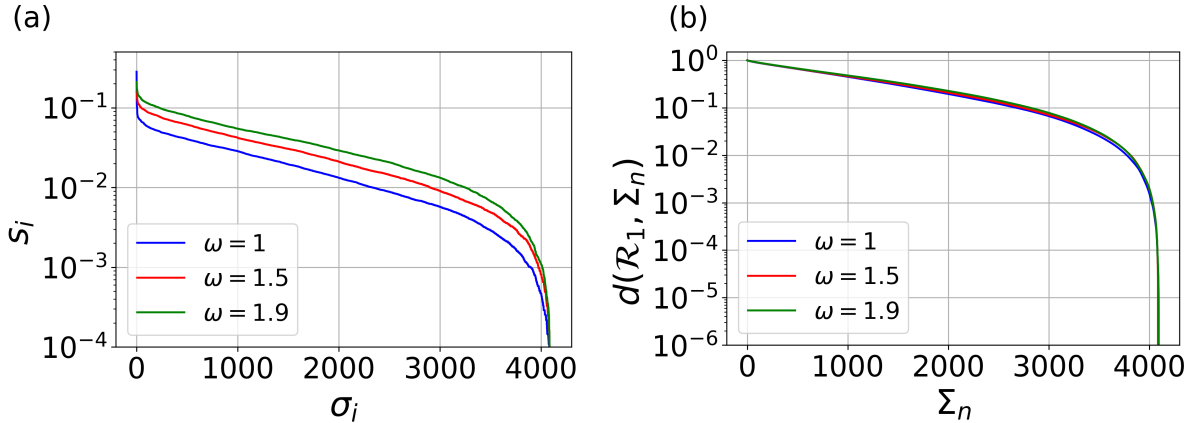


Figure 4. The expansion of the single lattice-site Carleman matrix \mathcal{R}_1 . In (a) the coefficients s_i of the expansion for each basis matrix σ_i . In (b) the normalized Frobenius distance d between matrix \mathcal{R}_1 and the approximation Σ_n obtained with the first n elements of the expansion.

As a result, standard techniques usually employed for Hamiltonian simulation such as low-order Trotterization²⁰ or linear combination of unitaries^{21,22} imply a depth of the associated quantum circuit that scales exponentially with the number of qubits¹¹, making the CLB scheme practically unviable. In the following we present a circuit for the CLB that overcomes this problem by employing block-encoding techniques²³ for sparse operators.

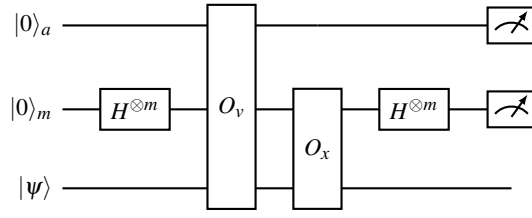


Figure 5. The circuit for the implementation of the dynamics using the block-encoding technique and matrix access oracles. Given a matrix \mathcal{C} , the operator \hat{O}_x is the position oracle which embeds the position of the non zero elements while \hat{O}_v is the value oracle which registers their values. If all the ancilla qubits are measured in the state $|0\rangle$, the state is proportional to $\mathcal{C}|\psi\rangle$, while any other combination leads to a different state, hence to an error.

V. BLOCK-ENCODING ORACLES

The depth problem of the circuit can be circumvented by using block-encoding for block-sparse matrices, namely by exploiting the sparse-matrix representation $(i, pos(i), v_{i,pos(i)})$, which encodes for each row i the position $pos(i)$ of the non null values $v_{i,pos(i)}$ for the matrix \mathcal{C} . With the block-encoding, we can define the non-unitary matrix \mathcal{C} as a block of a larger unitary operation $U(\mathcal{C})$, such that

$$U(\mathcal{C}) = \begin{pmatrix} \mathcal{C}/\gamma & \star \\ \star & \star \end{pmatrix}, \quad (21)$$

where $\gamma = \max_{i,j} |v_{i,j}|$ is the maximum value in \mathcal{C} , while the symbol \star represents elements that we can ignore, provided they satisfy the condition for U to be unitary. Thus, when applied to a state $|\psi\rangle$, the (normalized) evolution $\mathcal{C}|\psi\rangle$ is obtained when the ancilla qubits used for the block-encoding are measured in the state $|0\rangle$.

The block-encoding strategy^{23,24} requires the use of two extra quantum registers, labeled m and a , initialized in the state $|0\rangle$ and the use of two oracles operators, \hat{O}_x, \hat{O}_v as described next. The quantum register $|0\rangle_m$ consists of m ancilla qubits, where $m = \log_2 s$, s being the sparsity of the matrix (the maximum number of non-zero elements per row, for all rows in the matrix). It is used to store the position $j = pos(i)$, for each non zero entry $\mathcal{C}_{i,j}$ along the i -th row. Thus the oracle \hat{O}_x on the state $|i\rangle$ acts as follows:

$$\hat{O}_x|i\rangle|0\rangle_m = |i\rangle|pos(i)\rangle_m. \quad (22)$$

A second oracle \hat{O}_v , provides the value $\mathcal{C}_{i,pos(i)}$, by applying a controlled rotation onto an extra ancilla qubit:

$$\hat{O}_v|i\rangle|j\rangle_m|0\rangle_a = |i\rangle|j\rangle_m(\mathcal{C}_{i,j}|0\rangle_a + \sqrt{1 - \mathcal{C}_{i,j}^2}|1\rangle_a). \quad (23)$$

The circuit is plotted in Fig. 5.

The oracles take full advantage of the sparse nature of the Carleman matrix, which is particularly useful whenever the sparse matrix presents characteristics such as sorted position and values repetitions. For instance, a tridiagonal Toeplitz matrix can be mapped into a quantum circuit with just a polynomial depth.^{15,24}

This advantage comes at a cost, though. The nonunitary matrix \mathcal{C} is implemented only on the subspace where all the ancilla qubits are in the state $|0\rangle$, thus making the circuit probabilistic, with a success rate p_s that depends on the degree of non-unitarity of the Carleman matrix, as well as on the initial state $\sum_i c_i|i\rangle$. In fact, the equation of the success rate takes the form¹⁵

$$p_s = \frac{1}{2^{2m}} \left\| \sum_{i,l} c_i \mathcal{C}_{i,c(i,l)} |c_i, l\rangle \right\|^2. \quad (24)$$

However, the dominant contribution is the one due to the number of ancilla qubits used for the embedding, which dictates a success rate $p_s \approx \frac{1}{2^{2m}}$. In our case, m is proportional to the sparsity, which is given by the square of the number of discrete velocities $s = b^2$, leading to:

$$p_s \approx \frac{1}{2^{4 \lceil \log_2 b \rceil}} \approx \frac{1}{b^4}.$$

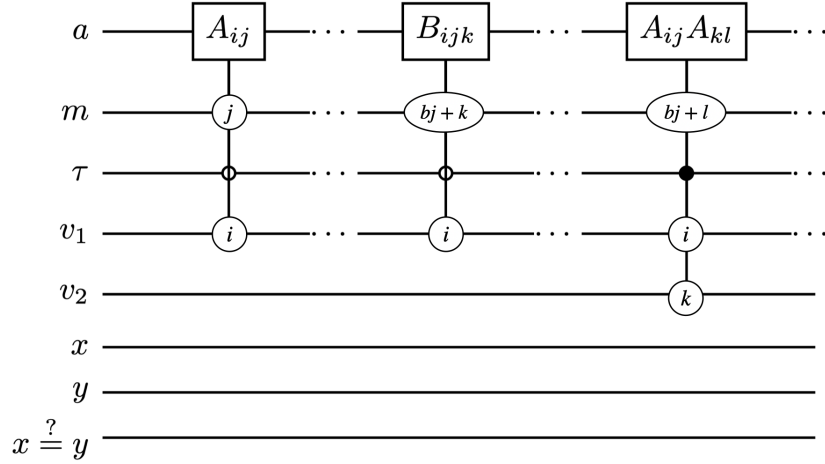


Figure 6. The value oracle \hat{O}_v for the D2Q9 LBM truncated at second order. A controlled rotation applies the value A_{ij} on the ancilla qubit a if the state in m is $|i\rangle$ the state in τ is $|0\rangle$ and the state in v_1 is $|j\rangle$. The same happens for the B_{ijk} and the $A_{ij}A_{kl}$ matrices. In this figure we followed the convention introduced in¹¹, where a circle including a number n implies a control conditioned by the state $|n\rangle$.

Taking into account the ceiling factor, this yields $p_s \approx 4 \cdot 10^{-3}, 6 \cdot 10^{-5}, 4 \cdot 10^{-6}$ for the D1Q3, D2Q9 and D3Q27 LB models, respectively.

For the D2Q9 model defined on a lattice with N sites, the relaxation matrix expressed in Eq. (19) has a sparsity $s = 81$, due to the second order term $A \otimes A$. Note indeed that both A and B are quite full, since A itself is a 9×9 matrix and B is a 9×81 matrix. However, the global sparsity of \mathcal{R} , which is a square operator with $9N + 81N^2$ rows, remains 81 regardless of the total number of lattice sites N .

We can exploit this property by using the matrix access oracles, that enable us to encode \mathcal{R}_N with $m = 7$ ancilla qubits, which results in a total number of gates scaling linearly with the size of the lattice.

The circuit acts on the quantum registers shown in Figs. 6 and 7, where a and m are the ancilla qubits used for the block-encoding, τ is a single qubit accounting for the truncation order, v_1, v_2 are the velocity registers with $\lceil \log_2 b \rceil$ qubits and x, y the position registers with $q_N = \lceil \log_2 N \rceil$ qubits. By using these quantum registers, the first order functions are encoded in the state $\sum_{i,x} f_i(x) |0\rangle_\tau |i\rangle_{v_1} |x\rangle_x$, whereas the second order functions are encoded in the state $\sum_{i,j} \sum_{x,y} f_i(x) f_j(y) |1\rangle_\tau |i\rangle_{v_1} |j\rangle_{v_2} |x\rangle_x |y\rangle_y$, both properly normalized and while the remaining qubits are in the state $|0\rangle$ if not specified otherwise.

A last single ancilla qubit is switched on when $x = y$, which is implemented through a comparator circuit U_- , which sets the $x = y$ ancilla qubit to $|1\rangle$ if $|x\rangle = |y\rangle$. The linear dependence of the depth with $\log_2 N$ for the relaxation operator comes from this comparator circuit. Fig. 6 shows the circuit for the values oracle. This applies controlled rotations on the value qubit a depending on the sparsity index m , the truncation order τ and the velocities v .

Fig. 7 shows the circuit for the position oracle. This is more cumbersome than the values oracle, as it uses different operators. S_+ is the rightward shift operator, and it is used to find the position of the diagonal blocks of \mathcal{R}_N , namely A and $A^{\otimes 2}$. The set operator accounts for the B on the off-diagonal blocks of \mathcal{R}_N , which comprises a limited number of CNOTs and single qubits rotations. This number is fixed, regardless of the number of gridpoints.

Hence, the circuit for implementing the relaxation term \mathcal{R}_N has a linear dependence with q_N , which is given solely by the comparator circuit U_- . At the same time, the circuit for implementing the streaming operator \mathcal{S} has a depth that is quadratic with q_N ^{11,25}, thus making the whole circuit gate complexity $\mathcal{O}(q_N^2)$.

We remind that the success probability of implementing a single time step for the D2Q9 model lies in the order of $p_s \approx 10^{-5}$. We performed the calculation to retrieve the exact probability distribution in the case of an initial state where all the velocity distributions are uniform, $f_i = \frac{1}{9}$, and in the case of no-flow equilibrium, with $f_i = w_i$ for $i = 0, \dots, 8$.

We found that in both cases the probability distribution has a maximum at $\omega = 0.31$, as shown in Fig. 8. This curve exhibits a cusp that stems from the renormalization that we need to apply to the matrices A and B , since the block-encoding technique is restricted to matrices with maximum values equal to 1, cf. Eq. (21). Fig. 8(a) shows the success probability for a single time-step for the uniform case and a number of lattice sites $N = 2^3$ (blue curve) and $N = 2^{10}$ (red curve). For higher values of N , the success probability is similar to the one obtained for the case $N = 2^{10}$. Fig. 8(b) shows the success probability for the equilibrium case. Here the result does not depend on the number of gridpoints, as it is expected from the equilibrium condition.

The use of block-encoding with oracles can provide an efficient circuit in terms of number of two-qubit gates necessary to implement a single time step. Clearly those results are shaded by the low value of the success probability. In the lookout and conclusion section we discuss some ideas that may help mitigating this problem by increasing the amplitude of the desired state.

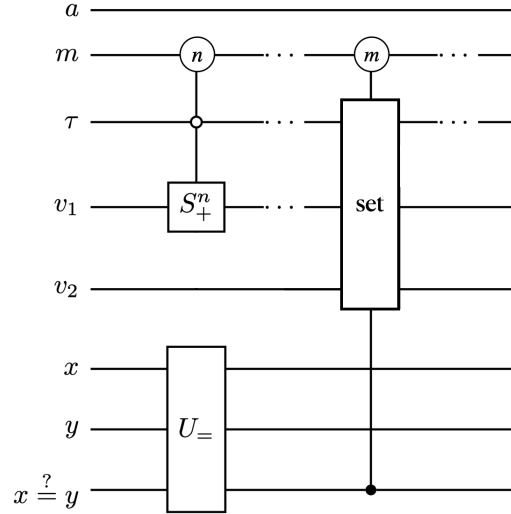


Figure 7. The position oracle \hat{O}_x for the D2Q9 LBM truncated at second order. Conditioned on the state of the m register $|n\rangle$, for $n = 0, 1, \dots, s$, we apply the shift operator S_+^m , which finds the position of the n -th element of the relaxation matrix \mathcal{R} . We do it both for $\tau = |0\rangle$ and $|1\rangle$. For $m = 0, 1, \dots, s$ and conditioned on the state $x = y$ being $|1\rangle$, we apply the *set* operator on the registers τ, v_1, v_2 , as described in the main text.

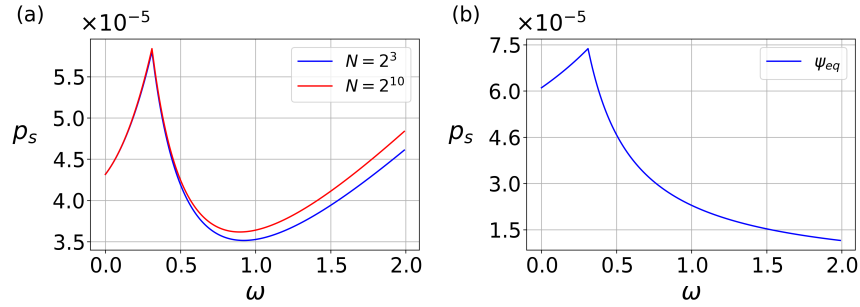


Figure 8. The success probability p_s of a single time step by using the block encoding technique as a function of ω obtained for (a) the uniform initial conditions $f_i = 1/9$ for each site, and (b) the equilibrium condition $f_i = w_i$ for each site.

VI. CONCLUSIONS AND FUTURE OUTLOOK

Summarizing, the classical implementation of the CLB procedure shows excellent convergence, at least for the 2D Kolmogorov flow discussed in this paper. In the quantum realm, a naive projection of the CLB matrix into the Pauli quantum gates faces with an exponential depth problem. Such an exponential depth can be brought down to a quadratic one by using block encoding oracles for block-sparse matrices. In this work we have developed the explicit form of the corresponding quantum circuit. However, this technique requires ancilla qubits, thus turning the quantum algorithm into a probabilistic one, whose success probability decays as the inverse of the forth power of the number of discrete velocities. For the case of the D2Q9 lattice this leads to a single-step success probability $p_s \sim 10^{-5}$, which makes the algorithm unviable on present day quantum computers. On the other hand, this probability is nearly independent of the number of lattice sites, a very appealing feature which would lead to a very efficient quantum algorithm once a way is found to boost the single-step success probability and bring it close to the unit value.

A natural candidate to this end is the oblivious amplitude amplification algorithm²⁶, which could in principle pull up the success probability close to the unit value. The challenge is then to develop a version of such an algorithm capable of handling non-unitary matrices. As an alternative, one could borrow ideas from the theory of open quantum systems, i.e. augment the LB equation with unitarity-restoring extra degrees of freedom. For instance one could add an extra population, g_i (mirror reservoir), obeying the same LB equation but with a collision term of opposite sign, so that the dynamics of the sum of the two, $h_i = f_i + g_i$, is collision free, hence unitary. One would then apply oblivious amplitude amplification to both f_i and g_i and focus the attention on f_i only. A second possibility is to expand the CLB matrix onto a second-quantized basis of annihilation and generation operators and apply block-encoding to each term in the expansion separately. The prospective advantage is twofold; first, the

expansion is likely to converge significantly faster than the Pauli basis expansion and second, each term is a one-sparse matrix, hence it can be implemented by the same block-encoding technique with a $O(1)$ success probability, since each matrix would require a single ancilla qubit. The challenge is to collect the cumulative effect of the various terms without losing efficiency.

A third (very optimistic) option is to analyse the nature of the errors introduced by the dissipative update, in the hope that they may display some sort of fault-tolerance or maybe even self-healing properties. This appears very unlikely, but a close investigation of the concrete effects of the failed dissipative updates on the dynamics of the quantum system may reveal unexpected features and possibly stimulate new ideas to increase the success probability.

All options above make an interesting topic for future work.

ACKNOWLEDGEMENTS

We acknowledge financial support from the Italian National Centre for HPC, Big Data and Quantum Computing (CN00000013) and from the NSF STAQ project under award NSF PHY-232580. One of the authors (SS) is grateful to the Physics and Astronomy Department of Tufts University for kind hospitality and financial support.

REFERENCES

- ¹R. Benzi, S. Succi, and M. Vergassola. The lattice Boltzmann equation: theory and applications. *Physics Reports*, 222(3):145–197, December 1992.
- ²Sauro Succi. *The Lattice Boltzmann Equation: For Complex States of Flowing Matter*. Oxford University Press, Oxford, New York, April 2018.
- ³M. Mendoza, B. M. Boghosian, H. J. Herrmann, and S. Succi. Fast Lattice Boltzmann Solver for Relativistic Hydrodynamics. *Physical Review Letters*, 105(1):014502, June 2010. Publisher: American Physical Society.
- ⁴Cyrus K. Aidun and Jonathan R. Clausen. Lattice-Boltzmann Method for Complex Flows. *Annual Review of Fluid Mechanics*, 42(1):439–472, 2010. [_eprint: https://doi.org/10.1146/annurev-fluid-121108-145519](https://doi.org/10.1146/annurev-fluid-121108-145519).
- ⁵Si Bui Quang Tran, Fong Yew Leong, Quang Tuyen Le, and Duc Vinh Le. Lattice Boltzmann Method for high Reynolds number compressible flow. *Computers & Fluids*, 249:105701, December 2022.
- ⁶Burkhard DÄijnweg and Anthony J. C. Ladd. Lattice Boltzmann Simulations of Soft Matter Systems. In Christian Holm and Kurt Kremer, editors, *Advanced Computer Simulation Approaches for Soft Matter Sciences III*, Advances in Polymer Science, pages 89–166. Springer, Berlin, Heidelberg, 2009.
- ⁷M.A. Nielsen and I.L. Chuang. *Quantum Computation and Quantum Information: 10th Anniversary Edition*. Cambridge University Press, 2010.
- ⁸Richard P. Feynman. Simulating physics with computers. *International Journal of Theoretical Physics*, 21(6):467–488, June 1982.
- ⁹Sauro Succi, W. Itani, K. Sreenivasan, and R. Steijl. Quantum computing for fluids: Where do we stand? *Europhysics Letters*, 144(1):10001, October 2023. Publisher: EDP Sciences, IOP Publishing and SocietÄ Italiana di Fisica.
- ¹⁰Wael Itani, Katepalli R. Sreenivasan, and Sauro Succi. Quantum algorithm for lattice Boltzmann (QALB) simulation of incompressible fluids with a nonlinear collision term. *Physics of Fluids*, 36(1):017112, January 2024.
- ¹¹Claudio Sanavio and Sauro Succi. Lattice BoltzmannÄCarleman quantum algorithm and circuit for fluid flows at moderate Reynolds number. *AVS Quantum Science*, 6(2):023802, April 2024.
- ¹²Wael Itani and Sauro Succi. Analysis of Carleman Linearization of Lattice Boltzmann. *Fluids*, 7(1):24, January 2022. Number: 1 Publisher: Multidisciplinary Digital Publishing Institute.
- ¹³C. Sanavio, R. Scatamacchia, C. de Falco, and S. Succi. Three Carleman routes to the quantum simulation of classical fluids. *Physics of Fluids*, 36(5):057143, May 2024.
- ¹⁴Claudio Sanavio, Enea Mauri, and Sauro Succi. Carleman-Grad approach to the quantum simulation of fluids, June 2024. [arXiv:2406.01118](https://arxiv.org/abs/2406.01118) [physics, physics:quant-ph].
- ¹⁵Claudio Sanavio, Enea Mauri, and Sauro Succi. Explicit Quantum Circuit for Simulating the Advection-Diffusion-Reaction Dynamics, October 2024. [arXiv:2410.05876](https://arxiv.org/abs/2410.05876).
- ¹⁶Jin-Peng Liu, Herman ÄYie Kolden, Hari K. Krovi, Nuno F. Loureiro, Konstantina Trivisa, and Andrew M. Childs. Efficient quantum algorithm for dissipative nonlinear differential equations. *Proceedings of the National Academy of Sciences*, 118(35):e2026805118, August 2021. Publisher: Proceedings of the National Academy of Sciences.
- ¹⁷Jin-Peng Liu, Dong An, Di Fang, Jiasu Wang, Guang Hao Low, and Stephen Jordan. Efficient Quantum Algorithm for Nonlinear Reaction-Diffusion Equations and Energy Estimation. *Communications in Mathematical Physics*, 404(2):963–1020, December 2023.
- ¹⁸Xiangyu Li, Xiaolong Yin, Nathan Wiebe, Jaehun Chun, Gregory K. Schenter, Margaret S. Cheung, and Johannes MÄijlmenstÄdt. Potential quantum advantage for simulation of fluid dynamics, April 2023. [arXiv:2303.16550](https://arxiv.org/abs/2303.16550) [physics, physics:quant-ph].
- ¹⁹Adriano Barenco, Charles H. Bennett, Richard Cleve, David P. DiVincenzo, Norman Margolus, Peter Shor, Tycho Sleator, John A. Smolin, and Harald Weinfurter. Elementary gates for quantum computation. *Physical Review A*, 52(5):3457–3467, November 1995. Number: 5.
- ²⁰James D. Whitfield, Jacob Biamonte, and AlÄn Aspuru-Guzik. Simulation of electronic structure Hamiltonians using quantum computers. *Molecular Physics*, 109(5):735–750, March 2011. Number: 5.
- ²¹Andrew M. Childs and Nathan Wiebe. Hamiltonian simulation using linear combinations of unitary operations. *Quantum Information and Computation*, 12(11&12):901–924, November 2012. Number: 11&12.
- ²²A. Mezzacapo, M. Sanz, L. Lamata, I. L. Egusquiza, S. Succi, and E. Solano. Quantum Simulator for Transport Phenomena in Fluid Flows. *Scientific Reports*, 5(1):13153, August 2015. Number: 1 Publisher: Nature Publishing Group.
- ²³Guang Hao Low and Isaac L. Chuang. Optimal Hamiltonian Simulation by Quantum Signal Processing. *Physical Review Letters*, 118(1):010501, January 2017.
- ²⁴Daan Camps, Lin Lin, Roel Van Beeumen, and Chao Yang. Explicit Quantum Circuits for Block Encodings of Certain Sparse Matrices. *SIAM Journal on Matrix Analysis and Applications*, 45(1):801–827, March 2024. Publisher: Society for Industrial and Applied Mathematics.
- ²⁵Adriano Barenco, Charles H. Bennett, Richard Cleve, David P. DiVincenzo, Norman Margolus, Peter Shor, Tycho Sleator, John A. Smolin, and Harald Weinfurter. Elementary gates for quantum computation. *Physical Review A*, 52(5):3457–3467, November 1995.

²⁶Dominic W. Berry, Andrew M. Childs, Richard Cleve, Robin Kothari, and Rolando D. Somma. Simulating Hamiltonian Dynamics with a Truncated Taylor Series. *Physical Review Letters*, 114(9):090502, March 2015. Publisher: American Physical Society.